

An AST/RO Survey of CO(4-3) in ultracompact HII regions

Wilfred M. Walsh¹

¹ *Harvard-Smithsonian Center for Astrophysics, 60 Garden St., MS-12, Cambridge, MA 02138*

wwalsh@cfa.harvard.edu

ABSTRACT

The Antarctic Submillimeter Telescope and Remote Observatory (AST/RO) has been used to observe 78 of the IRAS point sources identified by Bronfman et al. (1996) as likely ultracompact HII regions. Results for the CO $J = 4 \rightarrow 3$ line at 461.041 GHz are presented. The 74 sources detected are bright and in many cases compact, making them potentially suitable as pointing calibrators for single dish submillimeter telescopes.

1. Introduction

Most star formation (SF) occurs within the giant molecular cloud phase, and of particular interest is the behavior of the fragmented interiors of these clouds in the stages immediately before, during and after collapse into stellar objects. Both gaseous and dust components play vital roles in all SF models, and this paper presents submillimeter line observations of warm and dense gas near ultracompact HII regions, the ionized gas surrounding early-type stars. To identify the youngest stellar objects, far infrared (FIR) observations from the IRAS satellite's near all-sky survey have been used (Wood & Churchwell 1989) and follow-up line studies have successfully detected emission in many (sub)millimeter lines (e.g. Bronfman et al. 1996; Snell et al. 2000; Hatchell et al. 1998). Radio and IR continuum emission originates from ultracompact HII regions, while submillimeter line emission may come from hot molecular cores often found adjacent to one or more ultracompact HII regions. These objects are considered the best current tracer of ongoing SF.

An apparent problem with the understanding of ultracompact HII regions is that their dynamical ages appear to be so short ($\sim 10^4$ yr) that their numbers overpredict the current rate of SF. However the expected lifetimes depend critically on the local distribution of gas and dust (cf. Hollenbach et al. (1994); de Pree et al. (1995)), of which little is known. Recent interferometric observations (Walsh et al. 1998; Koo et al. 1996; Kurtz et al. 1999) suggest that at least some of the so-called ultracompact HII regions may in fact have larger sizes and predicted ages. Thus a better understanding of the distribution and dynamics of molecular gas and dust around ultracompact HII regions is required. In this paper we present results of a survey of 78 hot cores with the Antarctic Submillimeter Telescope and Remote Observatory. This survey is toward southern (Dec.

$\lesssim -20^\circ$ so as to be observable with AST/RO) sources in the list of Bronfman et al. (1996) with CS($2 \rightarrow 1$) emission and associated IRAS luminosity and colours typical of compact HII regions. The sources were further selected to have line profiles indicative of inward or outward motions (e.g., Mardones 1998) or have extended line wings which may indicate the presence of bipolar outflows. This database is likely to be representative of the early stages of massive SF. The results of this survey will be combined with observations of other submillimeter lines and continuum that will be analyzed in more detail in a subsequent paper but will also be of use to the several new southern submillimeter radiotelescopes as potential pointing and calibration sources. Published properties of bright, compact submillimeter sources in the southern sky are extremely sparse.

The observations are described in § 2 and in § 3 the data set is presented in the form of a table of spectral line parameters and as plots of the full spectra. Small maps of the brightest sources are also shown.

2. Observations

The observations were performed during the austral winter season of 2002 at the Antarctic Submillimeter Telescope and Remote Observatory (AST/RO; Stark et al. 2001), located at 2847 m altitude in Amundsen-Scott South Pole Station. This site has very low water vapor, high atmospheric stability and a thin troposphere making it exceptionally good for submillimeter observations (Chamberlin et al. 1997; Lane 1998). AST/RO is a 1.7 m diameter, offset Gregorian telescope capable of observing at wavelengths between $200 \mu\text{m}$ and 1.3 mm (Stark et al. 1997). The receiver used was a dual-channel SIS waveguide receiver (Walker et al. 1992; Honingh et al. 1997) for simultaneous 461–492 GHz and 807 GHz observations, with double-sideband noise temperatures of 320–390 K and 1050–1190 K, respectively. Telescope efficiency, η_ℓ , estimated using moon scans, skydips, and measurements of the beam edge taper, was 81% at 461–492 GHz and 71% at 807 GHz. The 807 GHz data will be presented, along with observations in several other bands, in a subsequent paper. Atmosphere-corrected system temperatures ranged from 700 to 4000 K at 461–492 GHz.

A beam switching mode was used, with emission-free reference positions chosen at least $20'$ from regions of interest, to make a small map of points surrounding each source. These maps were repeated as often as required to achieve suitable signal-to-noise. Emission from the CO $J = 4 \rightarrow 3$ and CO $J = 7 \rightarrow 6$ lines at 461.041 GHz and 806.652 GHz, (together with the [C I] $^3\text{P}_1 \rightarrow ^3\text{P}_0$ and [C I] $^3\text{P}_2 \rightarrow ^3\text{P}_1$ lines at 492.262 GHz and 809.342 GHz), was imaged over the 78 regions with a spacing of a half-beamwidth or less. The beam sizes (FWHM) were $103\text{--}109''$ at 461–492 GHz and $58''$ at 807 GHz (Stark et al. 2001).

Two acousto-optical spectrometers (AOSs; Schieder et al. 1989) were used as backends. The AOSs had 1.07 MHz resolution and 0.75 GHz effective bandwidth, resulting in velocity resolution of 0.65 km s^{-1} at 461 GHz and 0.37 km s^{-1} at 807 GHz. The data were smoothed to a uniform velocity resolution of 1 km s^{-1} . The high frequency observations were made with the CO $J = 7 \rightarrow 6$ line

in the lower sideband (LSB). Since the intermediate frequency of the AST/RO system is 1.5 GHz, the [C I] $^3P_2 \rightarrow ^3P_1$ line appears in the upper sideband (USB) and is superposed on the observed LSB spectrum. The local oscillator frequency was chosen so that the nominal line centers appear separated by 100 km s^{-1} in the double-sideband spectra.

The standard chopper wheel calibration technique was employed, implemented at AST/RO by way of regular (every few minutes) observations of the sky and two blackbody loads of known temperature (Stark et al. 2001). Atmospheric transmission was monitored by regular skydips, and known, bright sources were observed every few hours to further check calibration and pointing. At periodic intervals and after tuning, the receivers were manually calibrated against a liquid-nitrogen-temperature load and the two blackbody loads at ambient temperature and about 100 K. The latter process also corrects for the dark current of the AOS optical CCDs. The intensity calibration errors became as large as $\pm 15\%$ during poor weather periods.

Once taken, the data in this survey were reduced using the COMB data reduction package. After elimination of scans deemed faulty for various instrumental or weather-related reasons ($\lesssim 7\%$ of the total dataset), linear baselines were removed from the spectra in all species by excluding regions where the CS $J = 2 \rightarrow 1$ spectra of Bronfman et al. (1996) showed emission within twice the FWHM of Gaussian fits to the CS $J = 2 \rightarrow 1$ line. This allowed known emission to be readily excluded from the baseline fitting procedure.

While the original intent was to make T_{rms} as uniform as possible across all source maps, this was not always possible. For the CO $J = 4 \rightarrow 3$ transition, T_{rms} in 1 km s^{-1} wide channels with no spatial smoothing is on average $\lesssim 0.75 \text{ K}$.

3. Results

AST/RO’s pointing model (Stark et al. 2001) is currently determined by observing a small number of sources for a 24 hr period so as to obtain full coverage of the sky in azimuth. However these sources do not cover a wide range in elevation. As the residual pointing uncertainty after the application of the pointing model at AST/RO is between one beamwidth in the frequency used to determine the pointing model and one arcminute, it is a major aim of this work to identify a larger sample of compact sources, distributed over the sky, that may be used for pointing calibration. Therefore small images of a few square arcminutes were made of the sample with half-beam spacing. Fig. 1 displays the brightest spectrum observed in the vicinity of each source and Fig. 2 shows the resulting images.

Table 1 lists the results of Gaussian fits to the observed lines shown in Fig. 1. The first column is a shortened name based on the Galactic longitude, column two is the IRAS source name, columns three and four are the equinox J2000 coordinates. Column five is the peak antenna temperature as estimated by the Gaussian fit, with an uncertainty due to the fitting. The actual intensity calibration error of AST/RO is generally larger (§ 2). Columns six to eight are the central velocity,

integrated line intensity (in K km s^{-1}) and FWHM of the line as estimated by the Gaussian fitting, respectively. Fig. 1 shows that many of the line profiles can be approximately represented by a Gaussian form, leading to a reasonable estimate of the line strength, width and central velocity. The Gaussians, fit to a range of channels 10 km s^{-1} either side of the FWHM of the Bronfman et al. (1996) Gaussian fit to the CS $J = 2 \rightarrow 1$ line, clearly do not provide a precise model of the profiles, and further analysis of the spectra should refer to the original data, available online.

Fig. 1 shows that the great majority, 95%, of the sources are detected in the CO $J = 4 \rightarrow 3$ line and 86% of them have line strengths brighter than 5 K. Thus the CO $J = 4 \rightarrow 3$ line is a readily-detectable tracer of molecular material around ultracompact HII regions, and may be used as a kinematic tracer and for distance determination. The profiles are in nearly all cases characterized by a single component, whose V_{lsr} is in all but two cases the same as that of the CS $J = 2 \rightarrow 1$ line, within the fitting uncertainties. Those sources not detected at a level of several times the RMS noise per channel are indicated in the table as upper limits, the level of which is estimated to be 4.5 times the RMS per channel.

Images of a selection of the brightest sources detected in the CO $J = 4 \rightarrow 3$ line are shown in Fig. 2. The images were formed by simply summing the emission in channels within the FWHM of the Bronfman et al. (1996) Gaussian fit to the CS $J = 2 \rightarrow 1$ line. The images have been gridded onto a surface that over-samples the observed pointing centers by a factor of three using a Gaussian smoothing function with FWHM 30% larger than the beam, and weighted using cone interpolation with a similarly-sized interpolation radius. Bright molecular emission in the vicinity of ultracompact HII regions often originates from hot cores, which are expected to be relatively point-like compared with the AST/RO beam, except in those cases where an outflow is seen, where more than one molecular core is present, or if the dense molecular region is genuinely extended. Recent VLA results (Kurtz et al. 1999) show some ultracompact HII regions to lie within larger structures that may also contain extended molecular material. From Fig. 2 it can be seen that at least 50% of the sources in the present sample are unresolved by AST/RO and can potentially be used by single dish telescopes for pointing purposes.

The point-like images shown in fig. 2 can be used to select sub-samples for pointing purposes while extended structures may benefit from future mapping. These data will be combined with and analyzed in the light of measurements made in several other lines with a variety of opacities in a future paper.

Table 1. Results of AST/RO observations

Name	IRAS name	R.A. (J2000)	Dec. (J2000)	T _* ^A (K)	V _{lsr}	<i>I</i>	ΔV
G268.522	9028-4837	08:59:29.82	-48:13:17.31	2.8 ± 0.6 ^a	-	-	-
G269.854	9094-4803	09:11:08.40	-48:15:59.16	2.9 ± 0.5	78.8 ± 0.1	4.1	1.3
G281.586	10031-5632	10:04:56.23	-56:46:36.85	7.3 ± 0.1	-1.2 ± 0.1	45.2	5.8
G285.259	10295-5746	10:31:28.36	-58:02:07.47	23.3 ± 0.1	4.8 ± 0.0	129.9	5.2
G291.274	11097-6102	11:11:52.66	-61:18:35.38	25.3 ± 0.2	-20.9 ± 0.0	260.7	9.7
G297.725	11590-6452	12:03:22.80	-64:09:57.25	3.1 ± 0.8	-9.2 ± 0.1	2.3	0.7
G301.116	12331-6134	12:36:02.05	-61:51:05.41	9.6 ± 0.2	-39.0 ± 0.1	81.6	8.0
G301.134	12326-6245	12:35:33.87	-63:02:29.05	13.0 ± 0.2	-37.6 ± 0.1	87.0	6.3
G301.722		12:41:17.43	-61:44:10.45	10.9 ± 0.2	-38.6 ± 0.0	52.6	4.5
G301.731	12383-6128	12:41:17.42	-61:44:38.99	9.4 ± 0.3	-37.9 ± 0.1	53.9	5.4
G305.194		13:11:13.10	-62:44:56.10	11.7 ± 0.2	-33.9 ± 0.1	87.3	7.0
G307.559	13080-6229	13:32:30.47	-63:04:48.90	6.7 ± 0.2	-34.8 ± 0.1	28.2	3.9
G307.560	13291-6249	13:32:30.69	-63:05:17.36	7.3 ± 0.3	-33.4 ± 0.1	32.9	4.2
G309.920	13471-6120	13:50:41.53	-61:35:10.53	8.8 ± 0.3	-55.6 ± 0.1	31.2	3.3
G310.142	13484-6100	13:51:57.63	-61:15:45.78	7.9 ± 0.3	-54.9 ± 0.1	78.0	9.2
G312.599		14:13:13.88	-61:16:18.26	6.7 ± 0.2	-62.6 ± 0.1	47.0	6.6
G312.596	14095-6102	14:13:13.61	-61:16:47.12	6.2 ± 0.3	-60.8 ± 0.1	29.8	4.5
G318.047	14498-5856	14:53:41.34	-59:08:53.77	8.9 ± 0.2	-48.5 ± 0.1	65.7	7.0
G319.163	14593-5852	15:03:13.25	-59:03:53.96	6.9 ± 0.1	-20.4 ± 0.1	81.0	11.0
G320.674	15068-5733	15:10:43.24	-57:44:46.67	4.3 ± 0.3	-57.3 ± 0.1	19.4	4.3
G321.719	15100-5613	15:13:49.44	-56:24:55.02	7.9 ± 0.2	-39.6 ± 0.1	54.5	6.5
G322.933	15165-5524	15:20:21.12	-55:35:04.41	6.1 ± 0.6	-38.9 ± 0.1	6.6	1.0
G324.201	15290-5546	15:32:53.62	-55:56:12.40	8.9 ± 0.2	-85.7 ± 0.1	77.7	8.2
G326.466		15:43:17.74	-54:07:00.09	8.6 ± 0.1	-40.4 ± 0.1	108.6	11.8
G326.474	15394-5358	15:43:17.83	-54:07:32.62	7.5 ± 0.2	-38.9 ± 0.0	22.9	2.9
G326.655	15408-5356	15:44:42.79	-54:05:56.00	21.4 ± 0.2	-38.1 ± 0.0	224.8	9.9
G328.306		15:54:06.03	-53:11:07.59	2.0 ± 0.6	-8.9 ± 0.1	1.7	0.8
G328.307	15502-5302	15:54:06.01	-53:11:36.51	12.9 ± 0.2	-91.2 ± 0.1	116.2	8.5
G328.809	15520-5234	15:55:48.49	-52:42:40.20	3.4 ± 0.6	-101.3 ± 0.1	3.7	1.0
G329.337	15567-5236	16:00:32.89	-52:44:47.59	13.7 ± 0.0	-105.7 ± 0.0	94.8	6.5
G329.066	15573-5307	16:01:09.72	-53:16:01.76	4.9 ± 0.3	-47.3 ± 0.1	14.6	2.8
G329.404	15596-5301	16:03:31.25	-53:09:26.83	6.2 ± 0.3	-73.7 ± 0.1	36.0	5.5
G335.582	16272-4837	16:30:56.40	-48:43:46.39	3.7 ± 0.5	-66.4 ± 0.1	7.2	1.8
G330.883	16065-5158	16:10:21.83	-52:06:01.98	17.2 ± 0.2	-61.5 ± 0.0	132.0	7.2
G330.946	16060-5146	16:09:48.30	-51:54:52.36	8.7 ± 0.2	-88.3 ± 0.1	74.0	8.0
G331.126	16071-5142	16:10:56.83	-51:50:24.06	6.3 ± 0.2	-86.1 ± 0.1	42.5	6.4
G332.153		16:16:39.32	-51:16:28.40	10.6 ± 0.2	-54.9 ± 0.1	99.9	8.8
G332.293	16119-5048	16:15:45.15	-50:56:02.83	9.9 ± 0.3	-47.7 ± 0.0	31.5	3.0
G332.653	16158-5055	16:19:40.73	-51:03:10.97	11.3 ± 0.2	-47.4 ± 0.1	103.9	8.6
G332.831	16164-5046	16:20:14.28	-50:53:19.87	8.8 ± 0.2	-55.3 ± 0.1	117.7	12.6
G333.129	16172-5028	16:21:00.60	-50:35:19.84	22.4 ± 0.2	-50.5 ± 0.0	224.7	9.4
G333.306	16177-5018	16:21:30.61	-50:25:04.40	21.6 ± 0.2	-49.0 ± 0.0	225.1	9.8

I thank K. Brooks and G. Garay for suggesting the sample; K. Xiao, C. Martin and A. Stark for help with the observations; C. Walker and the receiver group at the U. of Arizona for their assistance; R. Schieder, J. Stutzki, and colleagues at U. Köln for their AOSs; J. Kooi and R. Chamberlin of Caltech, G. Wright of PacketStorm Communications, and K. Jacobs of U. Köln for their work on the instrumentation. This research was supported in part by the National Science Foundation under a cooperative agreement with the Center for Astrophysical Research in Antarctica (CARA), grant number NSF OPP 89-20223. CARA is a National Science Foundation Science and Technology Center. Support was also provided by NSF grant number OPP-0126090.

REFERENCES

- Bronfman, L., Nyman, L.-A., & May, J. 1996, *A&AS*, 115, 81
- Chamberlin, R. A., Lane, A. P., & Stark, A. A. 1997, *ApJ*, 476, 428
- de Pree, C. G., Rodriguez, L. F., & Goss, W. M. 1995, *Revista Mexicana de Astronomia y Astrofisica*, 31, 39
- Hatchell, J., Thompson, M. A., Millar, T. J., & MacDonald, G. H. 1998, *A&AS*, 133, 29
- Hollenbach, D., Johnstone, D., Lizano, S., & Shu, F. 1994, *ApJ*, 428, 654
- Honig, C. E., Haas, S., Hottgenroth, D., Jacobs, K., & Stutzki, J. 1997, in *Eighth International Symposium on Space Terahertz Technology*, 92
- Koo, B., Kim, K., Lee, H., Yun, M., & Ho, P. T. P. 1996, *ApJ*, 456, 662
- Kurtz, S. E., Watson, A. M., Hofner, P., & Otte, B. 1999, *ApJ*, 514, 232
- Lane, A. P. 1998, in *Astrophysics From Antarctica*, ed. G. Novack & R. H. Landsberg, Vol. 141 (ASP Conference Series), 289
- Mardones, D. 1998, Ph.D. Thesis
- Schieder, R., Tolls, V., & Winnewisser, G. 1989, *Experimental Astronomy*, 1, 101
- Snell, R. L., Howe, J. E., Ashby, M. L. N., Bergin, E. A., Chin, G., Erickson, N. R., Goldsmith, P. F., Harwit, M., Kleiner, S. C., Koch, D. G., Neufeld, D. A., Patten, B. M., Plume, R., Schieder, R., Stauffer, J. R., Tolls, V., Wang, Z., Winnewisser, G., Zhang, Y. F., & Melnick, G. J. 2000, *ApJ*, 539, L101
- Stark, A. A., Bally, J., Balm, S. P., Bania, T. M., Bolatto, A. D., Chamberlin, R. A., Engargiola, G., Huang, M., Ingalls, J. G., Jacobs, K., Jackson, J. M., Kooi, J. W., Lane, A. P., Lo, K.-Y., Marks, R. D., Martin, C. L., Mumma, D., Ojha, R., Schieder, R., Staguhn, J., Stutzki, J., Walker, C. K., Wilson, R. W., Wright, G. A., Zhang, X., Zimmermann, P., & Zimmermann, R. 2001, *PASP*, 113, 567

Table 1—Continued

Name	IRAS name	R.A. (J2000)	Dec. (J2000)	T _* ^A (K)	V _{ISR}	<i>I</i>	Δ <i>V</i>
G337.164	16351-4722	16:36:20.15	-47:24:29.43	4.5 ± 0.2	-65.0 ± 0.2	55.1	11.6
G337.703	16348-4654	16:38:33.29	-47:01:20.00	4.9 ± 0.3	-52.7 ± 0.2	34.8	6.7
G338.569	16385-4619	16:42:14.29	-46:25:28.13	10.2 ± 0.3	-114.6 ± 0.1	54.0	5.0
G339.622	16424-4531	16:46:06.65	-45:36:49.42	5.7 ± 0.2	-32.6 ± 0.1	40.2	6.6
G340.053	16445-4516	16:48:11.89	-45:21:32.25	9.1 ± 0.2	-51.0 ± 0.1	77.2	8.0
G340.248	16458-4512	16:49:30.26	-45:17:49.66	8.3 ± 0.2	-49.5 ± 0.1	71.0	8.0
G341.932	16510-4347	16:54:37.12	-43:51:55.92	7.0 ± 0.3	-42.0 ± 0.1	33.4	4.5
G342.697		16:56:04.02	-43:04:13.54	6.1 ± 0.4	-40.9 ± 0.1	25.8	3.9
G342.704	16524-4300	16:56:01.29	-43:04:43.95	5.5 ± 0.9	-41.2 ± 0.1	4.3	0.7
G343.126	16547-4247	16:58:16.90	-42:51:37.00	8.4 ± 0.5	-28.4 ± 0.1	25.4	2.9
G345.001	17016-4124	17:05:09.79	-41:28:34.07	6.5 ± 0.8	-85.7 ± 0.1	9.5	1.4
G345.208	16571-4029	17:00:35.41	-40:33:31.17	23.2 ± 0.3	-13.9 ± 0.0	133.9	5.4
G345.482		17:04:26.83	-40:45:57.05	21.4 ± 0.4	-17.2 ± 0.1	155.5	6.8
G345.490	17009-4042	17:04:29.50	-40:46:25.47	13.2 ± 0.3	-16.3 ± 0.1	117.2	8.4
G345.494	16562-3959	16:59:41.88	-40:03:44.10	19.3 ± 0.2	-10.8 ± 0.1	192.6	9.4
G345.499	17008-4040	17:04:20.41	-40:44:25.77	13.1 ± 0.3	-16.4 ± 0.1	71.1	5.1
G345.505	17008-4040	17:04:23.06	-40:43:56.31	21.9 ± 0.4	-17.1 ± 0.1	172.8	7.4
G345.717	16596-4012	17:03:06.30	-40:17:08.73	7.1 ± 0.6	-9.0 ± 0.1	13.6	1.8
G348.236	17149-3916	17:18:23.91	-39:19:10.19	16.6 ± 0.3	-10.8 ± 0.1	109.7	6.2
G348.534	17158-3901	17:19:16.17	-39:04:26.09	10.3 ± 0.2	-11.2 ± 0.1	117.0	10.7
G348.548		17:19:16.05	-39:03:55.67	22.9 ± 0.5	-11.0 ± 0.1	208.2	8.5
G350.103	17160-3707	17:19:26.32	-37:10:54.75	9.1 ± 0.2	-68.0 ± 0.1	124.2	12.8
G350.504	17136-3617	17:17:02.20	-36:21:08.60	3.1 ± 0.6	15.7 ± 0.2	5.7	1.7
G351.776	17233-3606	17:26:44.44	-36:09:26.63	9.1 ± 0.2	-1.4 ± 0.1	112.9	11.6
G352.630	17278-3541	17:31:13.88	-35:44:09.07	4.9 ± 0.2	-0.4 ± 0.2	62.9	11.9
G353.410		17:30:26.47	-34:41:09.16	26.5 ± 0.6	-15.0 ± 0.1	313.6	11.1
G353.416	17271-3439	17:30:28.87	-34:41:40.53	11.8 ± 0.3	-14.6 ± 0.1	153.8	12.3
G357.552	17385-3116	17:41:49.73	-31:18:22.66	14.1 ± 0.4	3.4 ± 0.1	54.0	3.6
G000.665	17441-2822	17:47:19.66	-28:23:08.21	4.5 ± 1.0 ^a	-	-	-
G005.633	17545-2357	17:57:33.60	-23:58:15.12	4.8 ± 0.9 ^a	-	-	-
G005.888	17574-2403	18:00:32.09	-24:04:02.75	18.5 ± 0.4	10.0 ± 0.1	123.9	6.3
G008.139	17599-2148	18:03:00.39	-21:48:04.92	7.8 ± 0.4	21.3 ± 0.2	44.6	5.4
G009.615	18032-2032	18:06:13.42	-20:31:47.22	9.3 ± 0.4	7.0 ± 0.1	58.8	6.0
G010.157	18064-2020	18:09:24.44	-20:19:27.99	7.4 ± 0.3	9.8 ± 0.3	107.6	13.7
G010.466	18056-1952	18:08:36.63	-19:52:03.35	6.9 ± 0.4	72.3 ± 0.3	62.6	8.5
G011.936	18110-1854	18:14:00.34	-18:53:22.22	5.0 ± 1.8 ^a	-	-	-

^aUpper limit: see text.

Stark, A. A., Chamberlin, R. A., Cheng, J., Ingalls, J., & Wright, G. 1997, *Rev. Sci. Instr.*, 68, 2200

Walker, C. K., Kooi, J. W., Chan, M., Leduc, H. G., Schaffer, P. L., Carlstrom, J. E., & Phillips, T. G. 1992, *Int. J. Infrared Millimeter Waves*, 13, 785

Walsh, A. J., Burton, M. G., Hyland, A. R., & Robinson, G. 1998, *MNRAS*, 301, 640

Wood, D. O. S. & Churchwell, E. 1989, *ApJS*, 69, 831

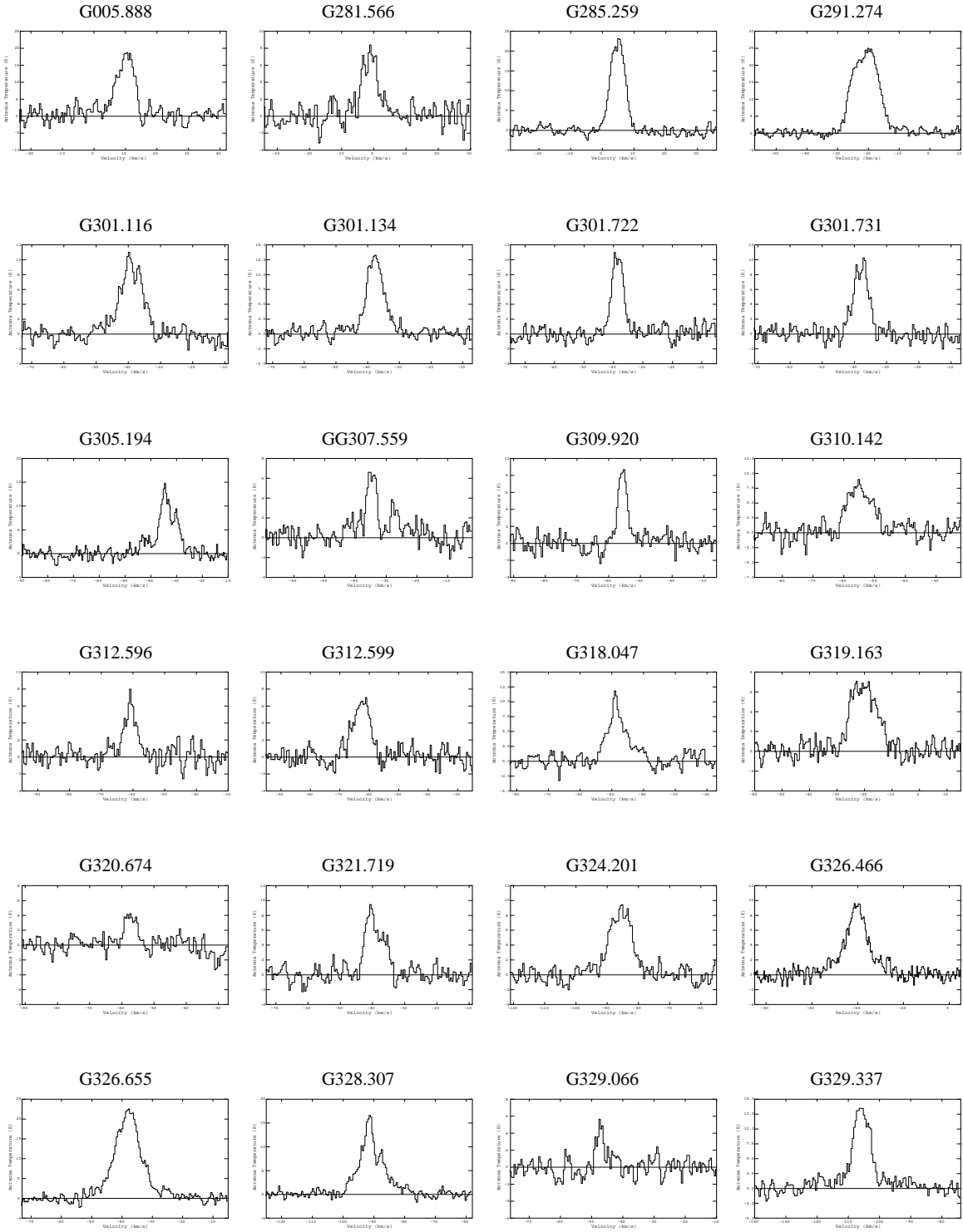


Fig. 1.— Spectra toward the sources listed in Table 1.

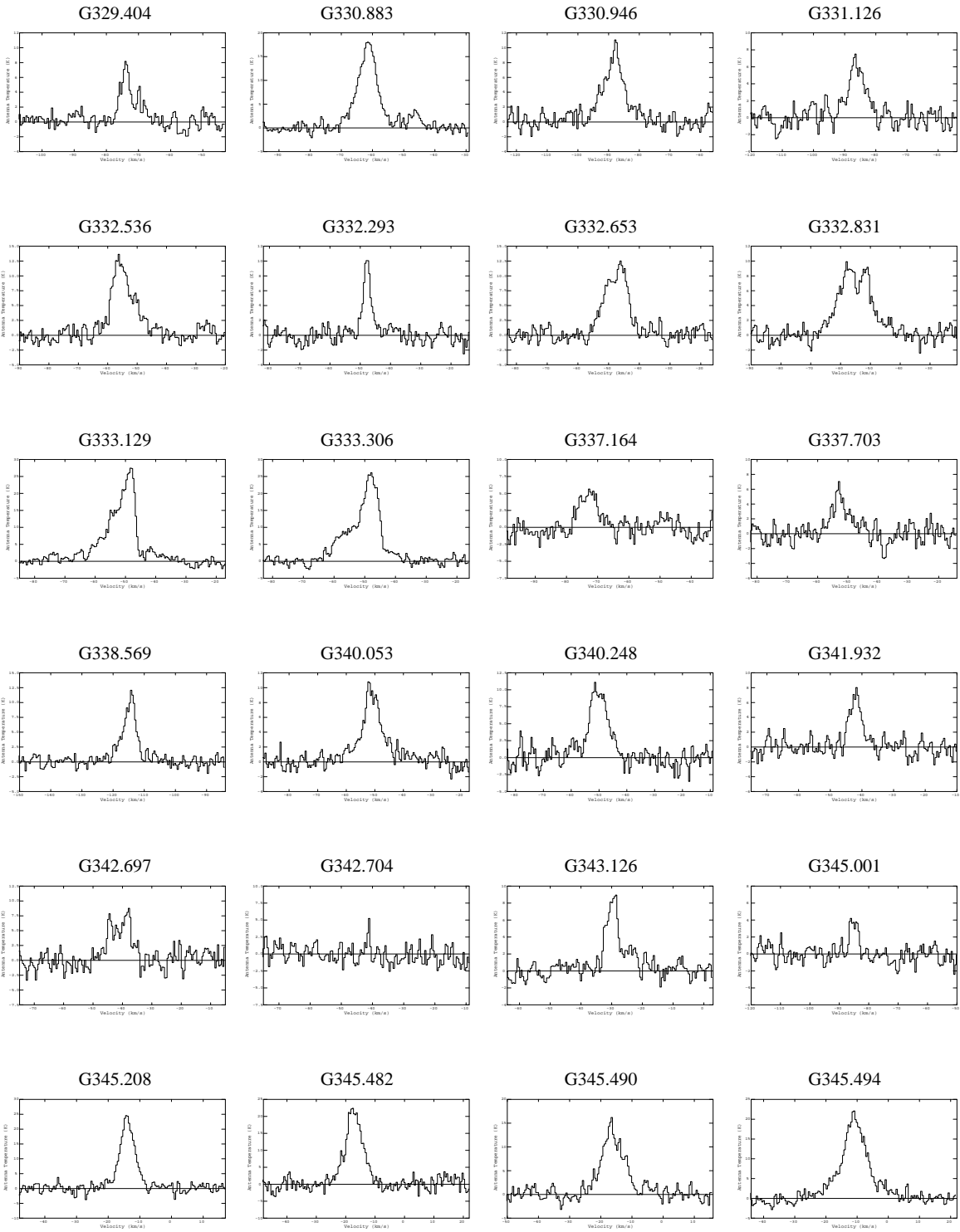


Fig. 1.— *Continued*

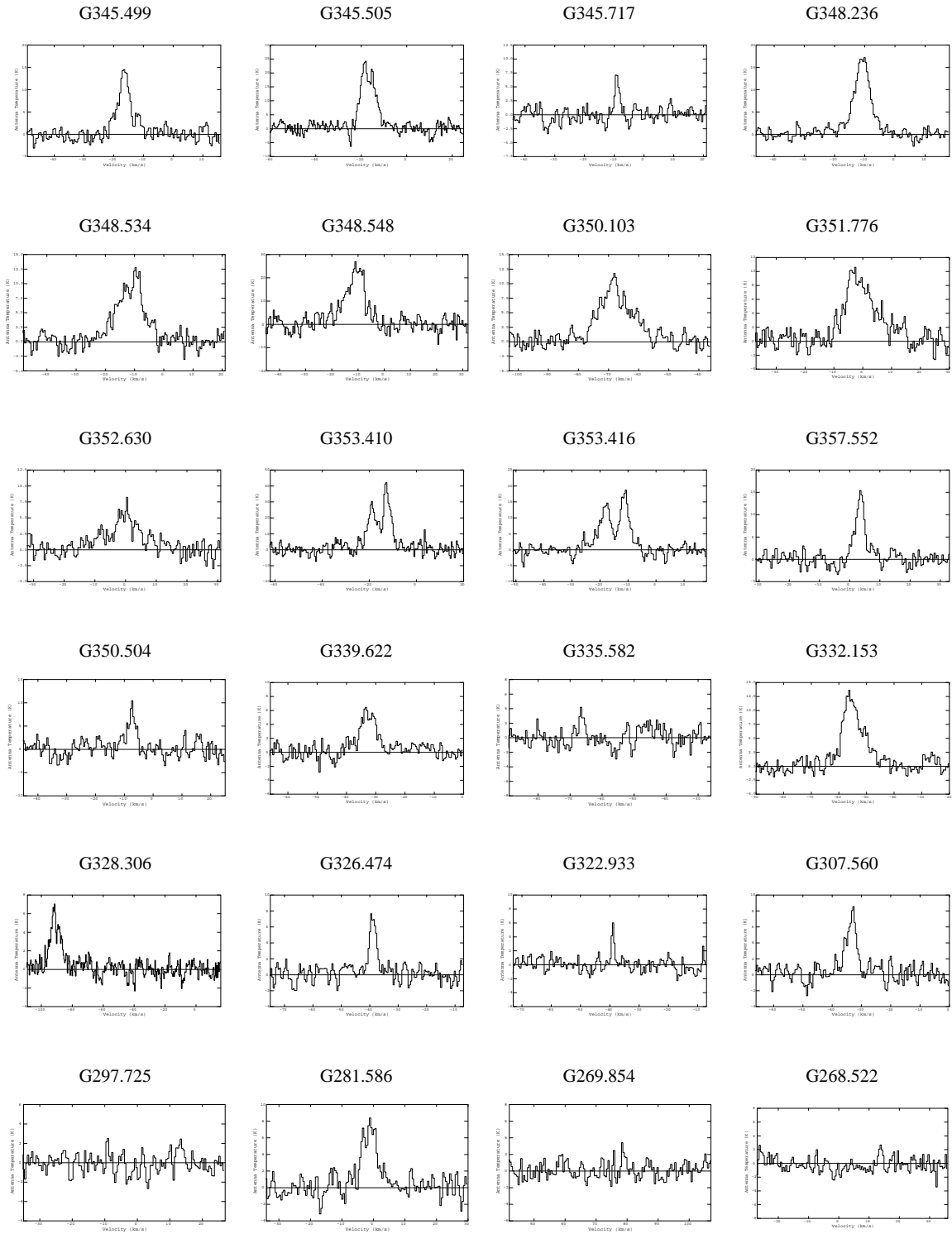


Fig. 1. — *Continued*

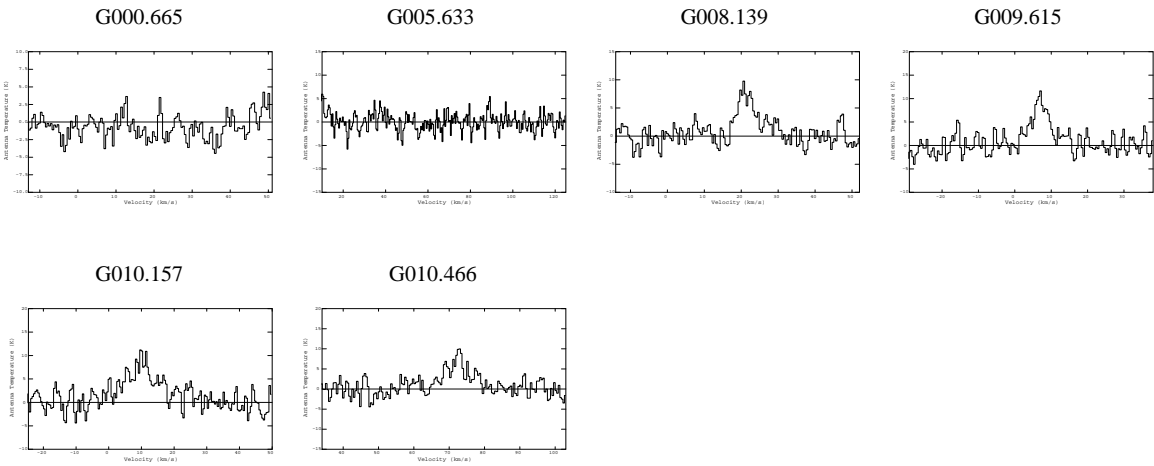


Fig. 1.— *Continued*

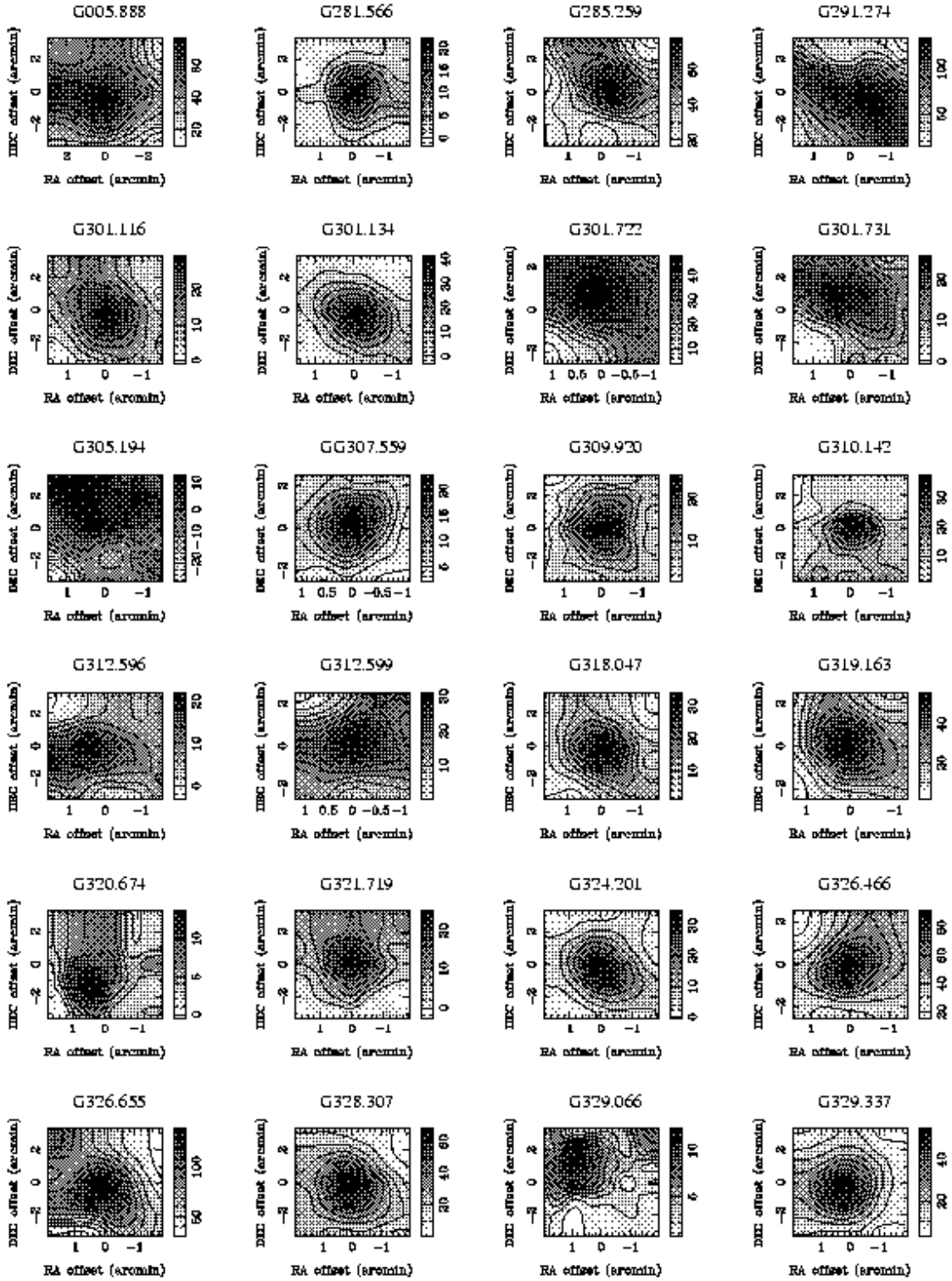


Fig. 2.— Images of the brightest hot cores in the CO $J = 4 \rightarrow 3$ line. The figures show the emission in the CO(4-3) line as both a greyscale and contours (5% to 95% of peak in 10% steps).

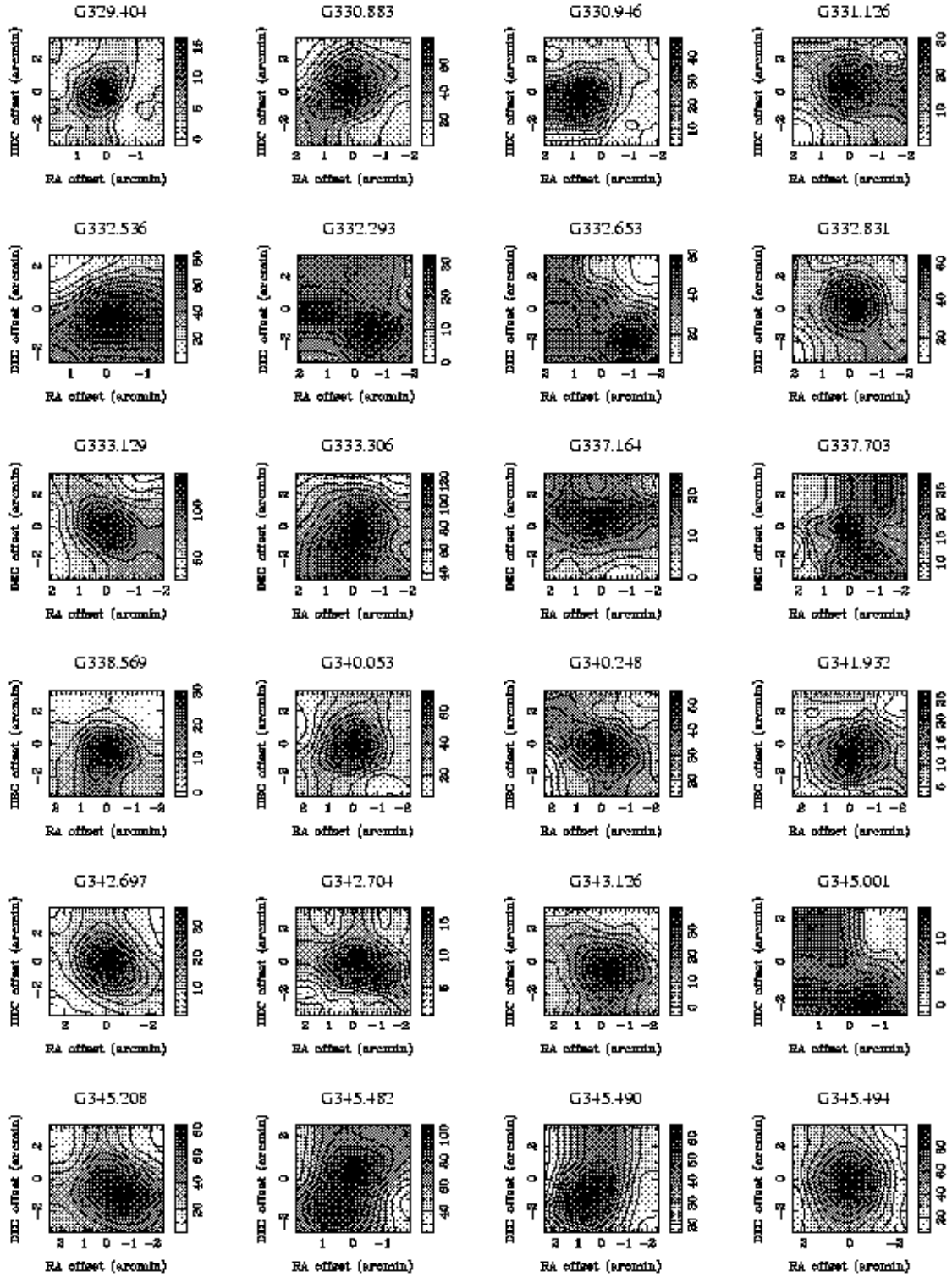


Fig. 2.— *Continued*

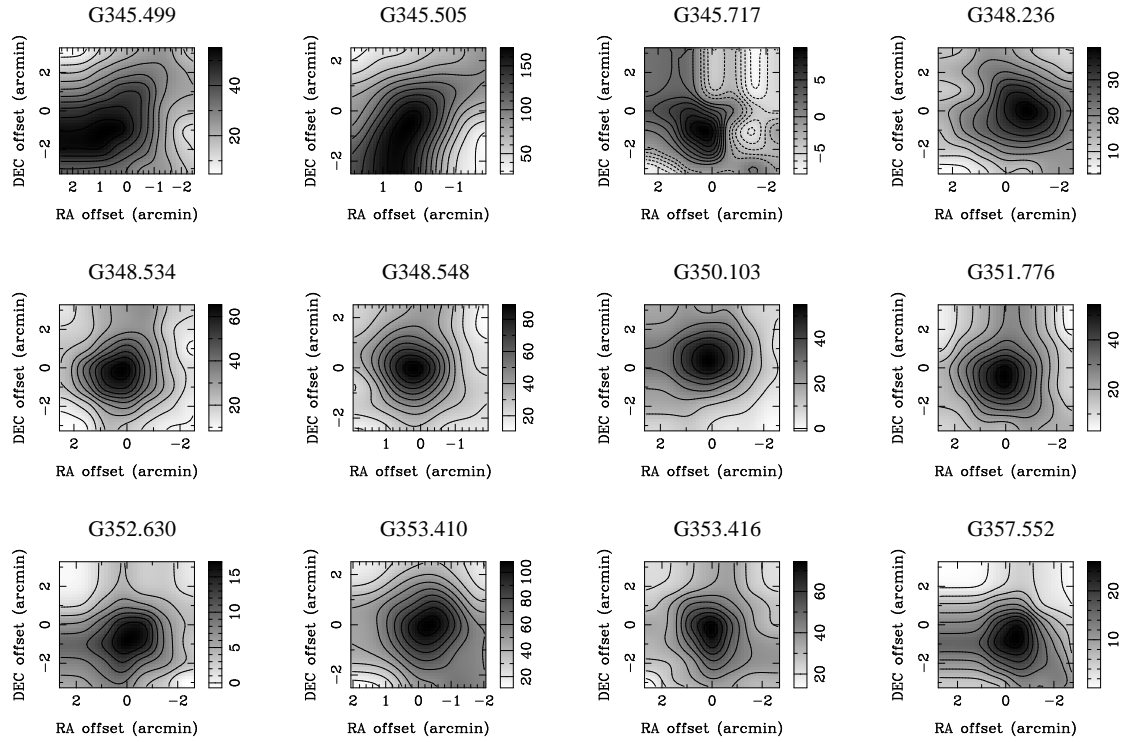


Fig. 2.— *Continued*